Draft version March 22, 2020
Preprint typeset using LaTeX style emulateapj v. 11/12/01

CAN WE PROBE THE ATMOSPHERIC COMPOSITION OF AN EXTRASOLAR PLANET FROM ITS REFLECTION SPECTRUM IN A HIGH–MAGNIFICATION MICROLENSING EVENT?

David S. Spiegel[1], Michel Zamojski[1], Alan Gersch[1,2], Jennifer Donovan[1], Zoltán Haiman[1]
[1]Department of Astronomy, Columbia University, 550 West 120th Street, New York, NY 10027
[2]Depertment of Astronomy, University of Maryland, College Park, MD 20742

dave@astro.columbia.edu, michel@astro.columbia.edu, agersch@astro.umd.edu, jen@astro.columbia.edu, zoltan@astro.columbia.edu

Draft version March 22, 2020

ABSTRACT

We revisit the possibility of detecting an extrasolar planet around a background star as it crosses the fold caustic of a foreground binary lens. During such an event, the planet's flux can be magnified by a factor of ~ 100 or more. The detectability of the planet depends strongly on the orientation of its orbit relative to the caustic. If the source star is inside the inter–caustic region, detecting the caustic–crossing planet is difficult against the magnified flux of its parent star. In the more favorable configuration, when the star is outside the inter–caustic region when the planet crosses the caustic, a close–in Jupiter–like planet around a Sun–like star at a distance of 8 kpc is detectable in 8-minute integrations with a 10m telescope at maximal $S/N \sim 15$ for phase angle $\phi \sim 10^\circ$. In this example, we find further that the presence of methane, at its measured abundance in Jupiter, and/or water, sodium and potassium, at the abundances expected in theoretical atmosphere models of close–in Jupiters, could be inferred from a non–detection of the planet in strong broad absorption bands at $0.6-1.4\mu$m caused by these compounds, accompanied by a $S/N \sim 10$ detection in adjacent bands. We conclude that future generations of large telescopes might be able to probe the composition of the atmospheres of distant extrasolar planets.

Subject headings: gravitational lensing – planetary systems – stars: atmospheres – stars:individual (HD209458) – astrobiology – astrochemistry

1. INTRODUCTION

With the first discovery a dozen years ago of a planet orbiting a star other than our Sun (Wolszczan & Frail, 1992), astronomy finally entered an age in which we could hope to answer scientific questions about distant planets, with the ultimate aim of detecting and characterizing an extrasolar Earth-like planet. Among the most tantalizing questions is: What is the chemical composition of an extrasolar planet? In this paper, we suggest a way to test for the presence of certain compounds in the atmospheres of extrasolar planets at much greater distances than has previously been discussed.

While the vast majority of the ~ 155 currently known extrasolar planets have been discovered in radial velocity surveys (e.g., see Marcy & Butler, 1998 or Woolf & Angel, 1998 for reviews [1]), two methods have recently been proposed to search for extrasolar planets via their gravitational microlensing signatures. These methods are complementary to the radial velocity surveys, in that they can detect planets at larger distances, well beyond our solar neighborhood, and one of these methods has the advantage of potentially providing information about the spectrum and therefore the composition of the planet (transit surveys have the same two advantages; e.g. Charbonneau et al. 2002).

Mao & Paczynski (1991) and Gould & Loeb (1992) suggest that as a background star passes behind a lens–star with a companion planet, the planet could be detected as lens, since it will cause a secondary, sharp spike in the source star's light–curve. Indeed, two years ago, a lens-plane planet was finally discovered (Bond et al., 2004). Recently, Graff & Gaudi (2000, hereafter GG00) and Lewis & Ibata (2000) have suggested that extrasolar planets might instead be detected in the source-plane, as they cross the caustics of a foreground lens system and are highly magnified relative to their parent star (Heyrovsky & Loeb 1997 also discuss from a theoretical perspective the possibility of using microlensing light–curves to probe structures in the source plane, in their case the structure of a background star behind a point–like lens, and other authors since then have carried out such studies, e.g. Albrow et al., 1999, Castro et al., 2001).

While detecting the planet as a lens, as Mao & Paczynski suggest, has the potential to reveal a statistically important sample of extrasolar planets, the drawback is that we receive no information about the planets except for perhaps their masses and projected separations from their host stars. Reflected light from a planet, however, contains information about physical parameters of the planet (presence and sizes of rings, satellites, spots and bands, for example). Detecting a planet as a lensed source therefore holds the promise of allowing these parameters to be measured, as suggested by Gaudi, Chang, & Han (2003, hereafter GCH03; Lewis & Ibata 2000 suggest further that polarization fluctuations during microlensing events could be indicative of properties of planetary atmospheres). In the present work, we investigate the viability of detecting an extrasolar planet as a microlensed source, and the extent to which a measurement of the magnified reflection spectrum can be used to glean information about the planet's atmospheric composition.

An unperturbed, isolated point–like lens (such as a single planet or a star) produces a point–like caustic. A binary lens, however, can produce a closed caustic curve, consisting of a set of piecewise concave curves that meet in cusps. In the present context, a binary lens, then, has several advantages over a point–lens: first, the relatively large spatial extent (compared to a point) of the binary lens caustic implies a much larger region in the sky in which for a high–magnification event to occur; second, since the caustic of a binary lens is a closed curve, caustic crossings come in pairs, and the second crossing can be anticipated; third, both star and planet can cross the caustic of a binary lens, while it is unlikely that both would cross the point–caustic of a point lens. When a background star with a

---

[1] For up–to–date information on the current status of these searches, see *http://www.obspm.fr/encycl/encycl.html* and *http://www.exoplanets.org.*

companion planet crosses the caustic of a binary lens, a unique observational signature will be produced in the light–curve. If such a signature is detected on ingress (or, if the lensed light–curve shows, at least, that the star has entered the inter–caustic region of a binary lens), GG00 suggest that many observatories could train their telescopes on this system so as to obtain dense sampling of the light–curve at egress (exiting the caustic region). If the planet's reflected light is sufficiently magnified, multi–color light–curves, or even detailed time-dependent spectra might, in principle, be obtained. Such spectral binning of the signal would shed light on the wavelength-dependence of the planet's albedo, which could in turn yield information about the chemical composition of the planet's atmosphere.

GCH03 suggest that morphological features such as moons or rings around extrasolar planets may be detectable, and they find a signal-to-noise ratio of ~ 15 for I-band detection of a planet in a typical planet-star-lens configuration with a 10m telescope. If the light (in a given wavelength range) is split up into N bands, the signal-to-noise ratio should go down roughly as $1/\sqrt{N}$. Signal-to-noise is also directly proportional to the diameter of the telescope's aperture. This suggests that with a 10m–class telescope, light could be split up into a few broad spectral bins before signal-to-noise becomes unacceptably low, and motivates us to examine whether useful information about the atmospheric composition of the planet could be obtained with this method.

The rest of this paper is organized as follows. In § 2, we present our model of a planetary caustic–crossing, including a detailed discussion of both the model of the planet and the computation of the caustic–crossing light–curve. In § 3, we discuss the detectability of extrasolar planets through microlensing. In § 4, we describe the albedos and reflection spectra of gas–giant planets in our own solar system. In § 5, we analyze the possibility of determining the wavelength–dependence of the albedo of a microlensed extrasolar planet. In § 6 we present a detailed discussion of the factors that affect the S/N of the detection of planets with various features in their reflection spectra. Finally, in § 7, we discuss the limitations of current technology, and conclude with projections of what may be possible with future instruments.

2. MODELING PLANETARY C<ruby><rb>AU</rb><rt>えー&

</ruby>STIC−CROSSING

2.1. *The Planet–Star System*

We consider a star with a companion planet as it crosses the fold–caustic of a binary lens. Figure 1 shows an illustration of the configuration we model. The observed surface–brightness of the planet at a given wavelength depends on properties of the star, the planet, and their relative geometry – specifically, the stellar flux, the albedo and phase of the planet, and the reflection or scattering properties of its atmosphere. For the stellar spectrum, we adopt that of a G0V star, and for the wavelength–dependent albedo of the planet's atmosphere, we use the gas giants in our own solar system as a guide (both to be described in more detail in § 4 below, where spectral features are considered). The planetary phase is given by the angle ϕ between the line–of–sight and the ray from the star to the planet (e.g. $\phi = 0°$ corresponds to the "full-moon" phase), as described in, e.g., GG00, GCH03, and Ashton & Lewis (2001). GCH03 adopted and compared two simple reflectance models (uniform and Lambert scattering) that prescribe the angular dependence of reflectivity; and Ashton & Lewis (2001) considered the effects of planetary phase. Neither of these studies, however, considered simultaneously the effects of the planet's phase and its reflectance model on the lensed light–curve. In our studies, we compared three different reflectance models: uniform, Lambert, and Lommel-Seeliger reflection (see, e.g., Efford, 1991 for more detailed discussions of these models, and see the Appendix for details on the computation of planet-models).

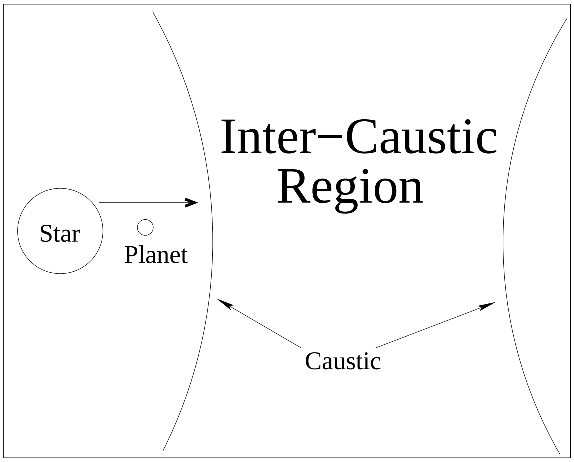

FIG. 1.— Schematic illustration of the planet–star system in the "planet–leading" configuration. The planet–star system is moving to the right, while the caustic stays still. In the reverse ("planet-trailing") configuration, the planet would be to the left of the star as they move to the right.

In Figure 2, we illustrate the surface brightness maps of three planets, one for each reflectance model described, each at fixed phase $\phi = 45°$. The maps were created numerically on a square grid of 401×401 pixels that we find to be sufficiently fine to converge on the light–curves we obtain below. We concur with GCH03 that with current technology it would be impossible to infer the true reflectance model of an extrasolar planet during a microlensing event, and so we use only one model, Lommel-Seeliger reflectance – which we expect to be the most realistic one, in calculating the light–curves that we present below.

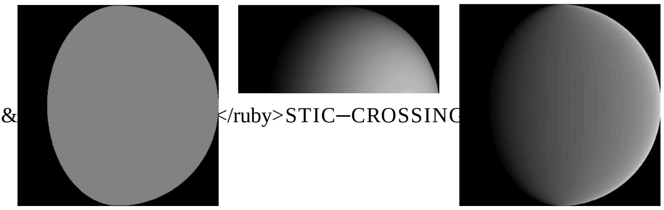

FIG. 2.— Illustration of the surface brightness of planets illuminated by a star at a phase angle of $\phi = 45$ degrees. The three panels assume different reflectance models. *Left panel:* uniform illumination; *Middle panel:* Lambert reflectance; *Right panel:* Lommel–Seeliger reflectance. The color maps differ slightly between the different models; all three scatter approximately equal amounts of light toward the viewer.

2.2. *Modeling the Caustic–Crossing Event*

For a good description of the details of gravitational microlensing, including see, for example, Mao & Paczynski (1991); for details regarding the generation and shape of fold-caustics, see GG00. We assume that the planet–star system described in § 2.1 above is in the source plane of a binary lens. The lensing stars are massive enough and close enough to one another that they generate a fold–caustic in the source-plane, a closed curve of formally infinite magnification. The caustic is considered to be a straight line (we follow GG00 and GCH03 and assume a low probability of crossing the caustic near a cusp) that sweeps across the planet and star. We assume that the plane of the planet's orbit is edge–on and is normal to the caustic at the point where the star-planet system crosses; we will argue in § 5 below that this simplification is not critical to our results. A source is magnified by the binary lens proportionally to the inverse square-root of the source's distance from the caustic when it is in the inter–caustic region (ICR) and not otherwise. We use the discretized magnification equation given by Lewis & Belle (1998) and Ashton & Lewis (2001):

$$\mathcal{A}_{\rm pix}(x_k) = 2\frac{\kappa}{\Delta x}\left(\sqrt{x_k+\Delta x}-\sqrt{x_k}\right)+\mathcal{A}_0, \qquad (1)$$

where $\mathcal{A}_{\rm pix}$ is the magnification of the pixel, κ is a constant close to unity that represents the "strength" of the caustic, Δx is the width of a single pixel, and x_k is the distance of the kth pixel from the caustic. In equations (1), distances are measured in units of the Einstein radius of the lens system: $\theta_E = \sqrt{2R_{\rm Sch}/D}$, where $R_{\rm Sch} = 2GM/c^2$ is the Schwarzschild radius of the lens, and $D \equiv D_{\rm os}D_{\rm ol}/D_{\rm ls}$ ($D_{\rm os}$, $D_{\rm ol}$, and $D_{\rm ls}$ are the distances between the observer and source, the observer and lens, and the lens and source, respectively). In our model, we use equation (1) to compute the brightness of each pixel across the face of the planet. We then sum the contributions from all of the 401×401 pixels to determine the total brightness at a given position x (corresponding to a given time during the lensing event).

2.3. *Preview of Results*

Using the model described above, we study a number of different scenarios. In all cases, we assume that the source star is a clone of HD209458, a G0V 8 kpc away with a companion planet that has the properties of HD209458b, i.e. a "Hot Jupiter," with radius $R_p = 1.35$ times the radius of Jupiter, and with orbital radius $a = 0.046$ AU (for details of the discovery of HD209458b, see Henry et al. 2000; Charbonneau et al. 2000). In order to reproduce the published results of GCH03, we assume generous viewing conditions with albedo $A = 1$ (all incident light is reflected). To model a more realistic situation, we examine several other albedo models, including Jupiter's albedo and a "gray atmosphere" – a constant, wavelength–independent albedo. The lens stars are assumed to be typical bulge stars, 6 kpc away, each with a mass of $0.3{\rm M}_\odot$.

We first consider a simple estimate of the flux from such a system. The un–magnified flux from a solar-type star 8 kpc away is quite low; $F_* = L_\odot/4\pi(8{\rm kpc})^2 \approx 5\times10^{-13}$ erg cm^{-2} s^{-1}. Since a typical photon ($\sim$ 500 nm) from such a star carries about 4×10^{-12} ergs, this flux corresponds to a photon number flux of approximately 0.1photons cm^{-2} s^{-1}. Even a large, close–in planet, such as the one under consideration, subtends a small solid angle from the star's perspective; so even with an albedo of $A = 1$, the flux of photons from the planet is reduced by a factor of $\gtrsim 10^4$ from the stellar flux. As a result, the flux from the planet is $\approx 6\times10^{-6}$ photons cm^{-2} s^{-1}. This is the well–known reason why gravitational microlensing is essential for detecting the reflected light of a planet around such a distant star.

Crossing a fold-caustic can lead to impressive magnification. In the situation under consideration, the Einstein radius of the lens is approximately 4000 times the radius of the planet, which means that, according to equation (1), a magnification factor of $\mathcal{A} \sim \sqrt{4000} \approx 60$ can be achieved.[2] As a result, as shown in the lightcurves below, the planet can perturb the total flux by as much as $\sim$ 1%.

Blending of background starlight in crowded fields makes detecting microlensing events more difficult. For details, see GG00 and GCH03. We follow GCH03 and ignore blending, for with good seeing its effect is negligible.

Note that the order in which the star and planet cross the caustic matters a great deal for the detectability of the planet. There are two basic ways in which the planet-star system can be configured as it crosses the caustic region – planet leading star or planet trailing star. Since a planet will almost surely not be detected on ingress, as the system enters the ICR, the favorable configuration for detecting a planet is the planet trailing the star on egress, so that the star is not magnified as the planet crosses the caustic. If the planet is leading the star on egress, the configuration is much less favorable for detecting the planet.

Finally, consider a future microlensing survey that uses a telescope large enough to discern the ingress signature of a planet crossing the caustic. Then, in a fraction of star-planet systems that cross fold-caustics, the system could be in the favorable configuration for both caustic–crossings (i.e., with the star outside the ICR when the planet crosses the caustic). This is because the ICR–crossing–time ($\sim 3-4$ days) is comparable to the semi-orbital period of a close-in extrasolar planet. For example, consider a planet with orbital period $\sim$ 6 days, twice the ICR–crossing time of $\sim$ 3 days. In this case, there should be a $\sim$ 50% chance that the planet will be in the planet-leading configuration on ingress and in the planet-trailing configuration on egress after having traversed half an orbit (and an equal chance of being unfavorably oriented both in ingress and egress); and so a planet *could* be detected on both ingress and egress. Clearly, the actual likelihood of catching the same planet on both ingress and egress crossings depends on the poorly known distribution of orbital radii for both the planets and for the binary lenses, but it is unlikely that the probability is negligibly small. While the coincidence between the orbital and intra-caustic-region-crossing timescales is interesting, we note that, in practice, a planet is unlikely to be detected on ingress – unless a deep future survey is devoted to blind monitoring of stars for lensing at $\sim$ hour time–resolution.

3. DETECTABILITY

Detecting the presence of a planet is, of course, challenging, since even when the planet is on the caustic, its flux is a small fraction ($\lesssim$ 1%) of even the un–magnified flux from the star. As an example, in the inset in Figure 3, we present a model R–band light–curve for a 10m telescope, showing first the star, and then the planet exiting the ICR in the favorable configuration for detecting the planet. The planet is modeled with Jupiter's albedo (described in §4 below), corresponding to $A \approx 0.45$. The solid dots show simulated data points. The broad peak between 0–2 hrs results from the star crossing the caustic. The three large dots at 3.0–3.3 hrs correspond to the planet crossing the caustic. On this scale, the magnified planetary flux is invisible against the un–magnified star-flux. Nevertheless, we next show that, as we suggest in § 2.3 above, with the current generation of 10m telescopes, it is possible to detect a planet when the star is outside the ICR (but not when the star is inside the ICR).

---

[2] Our calculations agree with those of Kayser & Witt (1989), and indicate that the maximum effective magnification of a uniform disk is $\sim 1.4/\sqrt{\rho}$, where ρ is the disk radius in units of the Einstein radius of the lens. The maximum effective magnification is slightly greater for Lambert and for Lommel-Seeliger scattering. Thus, an effective magnification factor of $\sim 1.5\times\sqrt{4000} \approx 100$ can be achieved.

In Figure 3, the top panel shows the tail of the light–curve (after the star has exited the ICR) for the planet's caustic–crossing egress at $\phi = 10^\circ$ (i.e. a zoom–in version of the planet signal from the inset). The bottom panel in this figure shows a random realization of the flux from the planet for the planet's caustic–crossing egress at $\phi = -45^\circ$ (i.e. in the unfavorable orientation). In both panels, we show error–bars corresponding to the $\sqrt{N}$ shot noise from the total photon–flux. (We ignore instrumental noise because shot noise will dominate for bright bulge stars.) We sum the signal and the $\sqrt{N}$ photon noise over five 8–minute integrations around the planetary caustic crossing. In the favorable orientation (the top panel), we find that the planet is detectable with a total $S/N \sim 15.3$ while in the unfavorable orientation, the planet is essentially undetectable ($S/N \sim 3.6$).

The relationship between the signal-to-noise of detection and the phase angle is summarized in Figure 4 below. The planet–flux/star–flux ratio is maximized when the planet is in the "full moon" phase ($\phi \sim 0^\circ$). When the star is outside the ICR, therefore, the planet's detectability is maximized for low phase angles. Phase $\phi \approx 10^\circ$ is optimal (the star intersects a fraction of the planet's surface for $\phi \lesssim 8^\circ$, leading to a rapid decrease in the S/N ratio for still smaller phase angles). When the star is inside the ICR, however, there is a more delicate balance. Since magnification in the ICR decreases with distance from the caustic, the planet's detectability is improved when the the projected impact parameter b is large, which happens for $\phi \sim \pm 90^\circ$. These two competing factors (planet–flux and star–flux) balance to maximize the planet/star flux ratio at about $|\phi| \sim 45^\circ$.

The reader can estimate from Figure 4 what fraction of the orbit will yield acceptable signal–to–noise. The S/N of detection exceeds 5 for approximately 90° of phase, or 1/4 of the orbit. Since we are inquiring what will be possible in good viewing conditions, we hereafter will consider only the favorable orientation ($\phi = 10^\circ$).

Note that, for most phases, the S/N of detection is decreased if the plane of the planet's orbit is inclined less than 90°, but is unaffected if the plane of the orbit is not normal to the caustic.

4. PLANETARY REFLECTION SPECTRA

HD209458 is one of a relatively small number of stars confirmed to have a transiting companion (HD209458b). By carefully comparing the spectrum of this star during a planetary transit against its spectrum outside transit, Charbonneau et al. (2002) measured how the opacity of the transiting planet's atmosphere varies with wavelength, and inferred the presence of sodium in the atmosphere. Performing a similar analysis, Vidal-Madjar et al. (2003) claim to find an extended hydrogen Lyα-emitting envelope surrounding the planet.

We here investigate the prospects of analogously observing, instead of a transmission spectrum during a transit event, a reflection spectrum during a caustic–crossing event. Although near–future ground–based coronographs (such as Lyot[3]) and more distant future space projects, such as the Terrestrial Planet Finder[4], will be able to probe the spectra of planets around nearby stars using coronographs or nulling interferometers (e.g., Kutchner & Traub, 2002), we are not aware of any other ways at this time to study the reflection spectra of extrasolar planets. We emphasize that the technique we present in this paper is not in competition with current coronographic work, but is rather in several senses complementary (for more information on coronographic techniques, see, e.g., Oppenheimer et al. 2001). First, current and near–future coronographic studies are not sensitive to close–in planets, because these planets lack sufficient angular separation from their host–stars, but these are precisely the planets that are most readily seen in the source–plane of a microlensing event. Second, the population of planets available to microlensing is in the Galactic bulge, or at a distance ~ 8 kpc, and is therefore complementary to the nearby population of planets that will eventually be available to the other methods just mentioned.

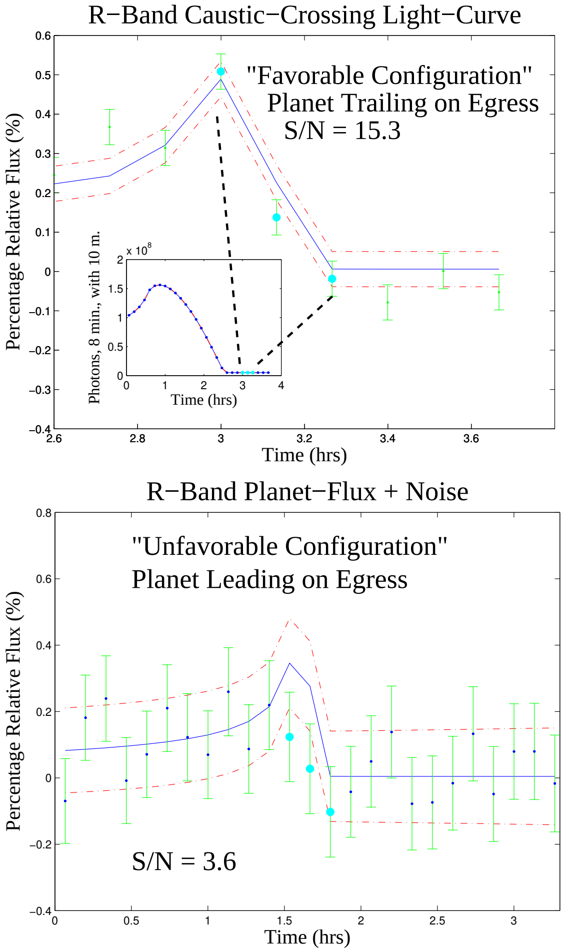

FIG. 3.— Planetary lensing light–curves on egress in the R-band, assuming Lommel–Seeliger reflection off a planet similar to HD20y9458b and with Jupiter's albedo, expressed as percentage change in the total flux caused by the presence of the planet. Solid (blue) curves show theoretical light–curves; dashed (red) curves show 1-σ errors; solid (blue) dots show random mock data (theoretical light–curve plus noise) with 1-σ error bars; large (cyan) dots denote times when the planet's surface intersects the caustic. *Top panel:* Favorable (planet–trailing) orientation for detection of the planet on egress. The inset shows the entire caustic-crossing lightcurve for both the star and the planet, with the ordinate showing total photons collected in 8 minute observations with a 10 m. telescope; the big plot is a zoom-in of the tail end of the inset. Dashed lines indicate the relationship between the inset and the parent image. An optimal phase angle of $\phi = 10^\circ$ was assumed. *Bottom Panel:* Unfavorable (planet–leading) orientation on egress, with the optimal value of $\phi = -45^\circ$.

As a first step toward modeling the reflection spectrum of an extrasolar planet around a solar-type star, we adopt the reflection spectra of the Jovian planets in our solar system, because these are the only gas-giant planets whose wavelength-dependent albedos have ever been measured. Atmospheric conditions, and hence reflection spectra, of hot Jupiters (extrasolar

---

[3] http://lyot.org

[4] http://planetquest.jpl.nasa.gov/TPF/tpf_index.html

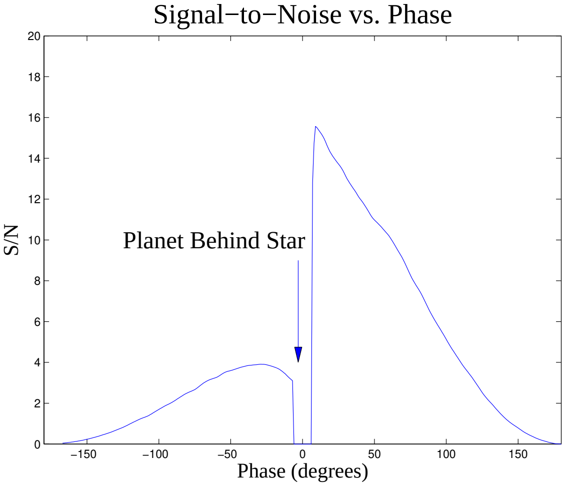

FIG. 4.— This figure shows the dependence of S/N on phase angle for R-band detection of a planet in a clone of the HD209458 system at 8 kpc, lensed by binary 0.3 $M_{\odot}$ stars at 6 kpc, in 8-minute integrations with a 10 m telescope. The plane of the planet's orbit is assumed to be inclined 90° to the line-of-sight (edge–on) and normal to the fold-caustic at the point of crossing. Typical proper-motion of lens and source (e.g. GCH03) is assumed. Since the plane of orbit is at inclination 90°, the planet disappears behind the star for phase angles $|\phi| \lesssim 8°$ and detectability drops to zero.

giant planets with short orbital periods) are likely to be much different from those of Jupiter, Saturn, Uranus, and Neptune (for detailed discussions of hot Jupiter atmosphere models, see, e.g., Sudarsky, Burrows, & Hubeny, 2003; Burrows, Sudarsky, & Hubeny, 2004; and Seager, Whitney, & Sasselov, 2000). However, given the uncertainty and differences among published atmospheric models of extrasolar giant planets, we prefer to base our calculations on the unambiguously measured albedos of the solar–system gas giants. We will then discuss (at the end of § 5 below) the expected differences for the hot–Jupiter atmospheres, and identify features in the theoretical spectra that could be detected at a similar significance.

To obtain our desired reflection spectra, we need the spectrum of a G2V star, and the albedos of the gas giants in our solar system (with albedo defined as the ratio of reflected flux to incident flux). We obtained an incomplete G2V spectrum from Greg Bothun's webpage[5], that had data missing at wavelengths of strong atmospheric absorption. Regions of missing data up to 1050 nm were filled in with a best-fit $T = 6000$ K blackbody spectrum, and the spectrum was normalized to a peak value of unity for clarity of presentation (see Fig. 5). Planetary albedos are taken from Karkoschka (1994), interpolated on a cubic spline (every 5nm) to the G2V reference wavelengths, and are shown for the four gas giants in Figure 6. Reflection spectra (in arbitrary units), then, are just the product of the albedo and the solar spectrum (shown by the bottom curve in Fig. 5).

While a reflection spectrum of an extrasolar planet with a high signal-to-noise ratio, covering a full range of wavelengths from the visible into the near infrared (NIR), would be ideal (see discussion in § 5 below), certain bands of the visible and NIR spectrum provide more information about chemical composition than others. By comparing the reflected flux from wavelength ranges where Jupiter's albedo is low with reflected flux from comparable wavelength ranges where Jupiter's albedo is much higher, we can infer the presence of those compounds

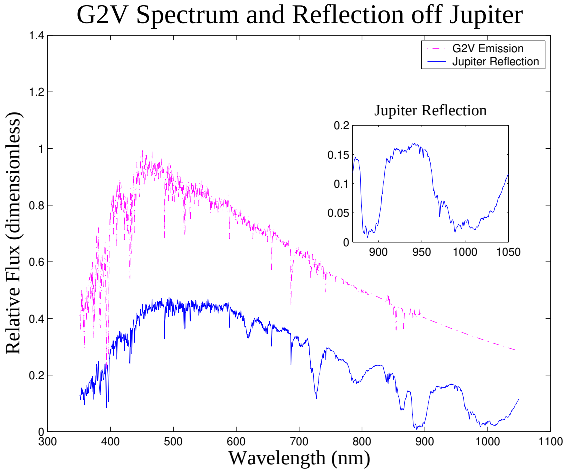

FIG. 5.— Spectrum of a G2V star (top, dashed-dotted magenta curve) and reflection spectrum of a G2V off a planet with Jupiter's albedo (bottom, blue curve). Inset: zoom–in of Jupiter's reflection spectrum over the wavelength range 870–1050nm.

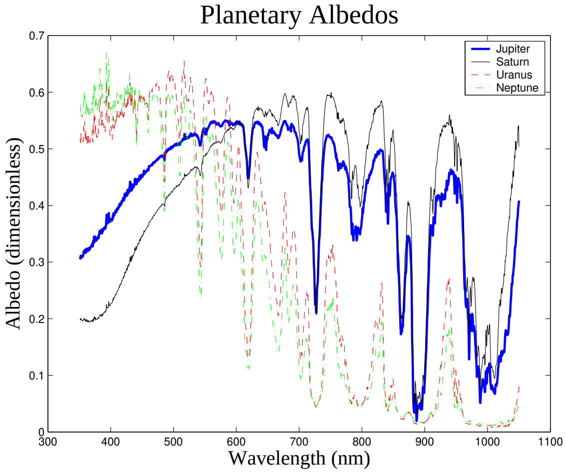

FIG. 6.— Albedos of Jupiter (thick blue curve), Saturn (thin black curve), Uranus (dashed red), and Neptune (dashed-dotted green), adopted from Karkoschka (1994).

responsible for the low albedo. It is clear from the bottom (blue) curve in Figure 5 that in a narrow band around 900nm (880nm-905nm) and in a slightly wider band around 1000nm (980nm-1030nm), Jupiter's albedo is quite low (~ 0.05 and ~ 0.1, respectively); while in–between (920nm-950nm), its albedo is much higher (~ 0.45). These troughs are caused by absorption by methane in the Jovian atmosphere (Karkoschka 1994). This stark contrast in albedo between adjacent wavelength bands suggests a way to search for, e.g., methane (or other elements or compounds that are expected, in theoretical models for hot Jupiters, to cause features with a similar equivalent width; see discussion below) in the atmosphere of an extrasolar planet.

We note that extrasolar giant planets can orbit very close to their host star (0.05 AU or less), but thermal emission from a planet would nevertheless contribute negligibly to the reflected flux at wavelengths $\sim 1\mu$m even for a hot planet (~ 1500K).

5. MODELING SPECTRA DURING CAUSTIC−CROSSING

If the (unlensed) flux from the star has spectrum $F_*(\lambda)$ and the planet has wavelength-dependent albedo $A(\lambda)$, then the flux

---

[5] *http://zebu.uoregon.edu/spectrar.html*

from the planet may be written

$$F_p(\lambda,t) = F_*(\lambda)A(\lambda)f(t), \tag{2}$$

where the multiplicative function $f(t)$ depends on various geometrical factors (the solid angle that the planet subtends from the perspective of the star, whether the planet has moons or rings, how far the planet is from the caustic, etc), and also on the reflectance model. The total observed flux, therefore, can be written (in the favorable orientation, with the star un–magnified, as discussed above) as

$$\begin{aligned} F_T(\lambda,t) &= F_*(\lambda)+F_p(\lambda,t) \\ &= F_*(\lambda)(1+A(\lambda)f(t)). \end{aligned} \tag{3}$$

The observables are F_T and F_*. The physically interesting characteristics of the planetary system, however, are $A(\lambda)$ and $f(t)$, and these may be solved for as

$$A(\lambda)f(t) = \frac{F_T(\lambda,t)}{F_*(\lambda)} - 1 \equiv G(\lambda,t), \tag{4}$$

where we define the function G as the observable quantity constructed on the right–hand side of equation (4). With perfect data, the time-difference between the star's and the planet's caustic crossings breaks the apparent degeneracy between A and f in the general solution,

$$A(\lambda) = k_1 \exp\left[\int \frac{\partial G/\partial\lambda}{G} d\lambda\right] \tag{5}$$

$$f(t) = k_2 \exp\left[\int \frac{\partial G/\partial t}{G} dt\right], \tag{6}$$

(where k_1 and k_2 are constants of integration such that $Af = G$).

In practice, with data as noisy as can be expected with the current generation of telescopes, it is impossible to separate A from f, and A may be determined only given a model for f. Still, it is possible in principle to posit a model for f (as outlined in § 2 above) and then to solve for $A(\lambda)$. In this case, since the signal–to–noise ratio for the detection of the planet we find is only ~ 15.3, it is still only possible to split the light into a few broad spectral bands, rather than into a resolved spectrum.

In order to test the idea that we could look for the spectral signature of a particular compound in the reflected light from a distant extrasolar planet, we model a planet with Jupiter's reflection-spectrum and scrutinize the model data for evidence of methane. In order to maximize signal–to–noise, we assume an egress caustic–crossing with planetary phase $\phi = 10°$.

To search for signatures of methane, we construct a mock "methane band filter (hereafter "MBF"), that allows complete transmission from 880nm-905nm *and* from 980nm-1030nm (the bands where Jupiter's albedo is low because of methane, as discussed in §4) and zero transmission elsewhere (MBF is therefore a "double top-hat" filter). Note that we do not necessarily mean a physical filter here; we effectively assume that the flux in a low-resolution spectrum can be binned and computed in these wavelength ranges. A more realistic analysis would have to take into account the additional instrumental noise in any physical implementation of such a filter (such as read–out noise in the case of a spectrograph). We then compare the MBF light–curve of a model planet with Jupiter's albedo to the MBF light–curve of a model planet with the methane feature removed – i.e., a model planet where the albedo is replaced by a constant equal to Jupiter's mean albedo $\bar{A} = 0.45$. Figure 7 shows this comparison: the top panel shows the MBF light–curve for a planet with Jupiter's albedo (here, the planet is detected at $S/N = 1.8$, which counts as a non-detection); the bottom panel shows the MBF light–curve for a planet with constant albedo $A = 0.45$ (here, the planet is detected at $S/N = 8.4$).

In practice, the observational strategy would involve employing a "high albedo filter" (hereafter "HAF") that uses a region of the spectrum that is relatively unaffected by methane and that is comparable in width to the MBF filter (e.g. the adjacent 920nm-950nm region, and/or other regions where Jupiter's albedo is high). The flux measured through the HAF filter would then be used to predict the expected MBF flux according to the no–methane null–hypothesis. In practice, then, a *non*–detection of the planet in the MBF band together with a simultaneous *detection* in the HAF band, would be evidence for the presence of methane in the atmosphere of the planet. The S/N is proportional to the square root of the number of photons collected, and to the diameter of the telescope. With a future 30 or 100m telescope, therefore, it would be possible to achieve a S/N of ~ 25 or ~ 80, respectively, in detecting the presence of methane.

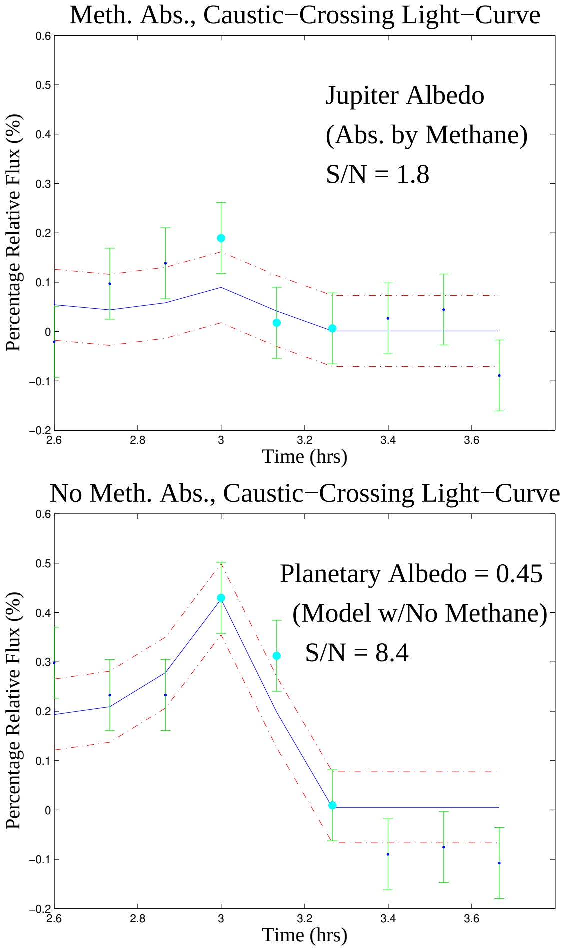

FIG. 7.— Egress light–curves in the MBF band, which covers two deep methane absorption features and includes light from 880nm-905nm and from 980nm-1030nm. The meaning of the symbols are as in Figure 3. *Top panel:* Jupiter's low albedo is adopted, which leads to a non–detection of the planet. *Bottom panel:* A constant albedo of $A = 0.45$ is used showing what the light–curve would look like if there were no methane present ($S/N = 8.4$). This plot is quite similar to the light–curve that would be obtained through a filter in a band where there is low methane absorption and Jupiter's albedo is much higher ($\sim 0.4 - 0.5$).

6. DISCUSSION

Note that, strictly speaking, our S/N calculations are for a space-based observatory, because we do not include sky brightness. Detailed data on sky brightness are available in Lienert et al. (1998). In R-band, the contribution to total flux from the sky is small for good seeing (for seeing $\sim 0.75''$, the star is more than an order of magnitude brighter than the sky within the aperture subtended by the star). At 900nm, the star is still several times brighter than the sky for good seeing conditions, but by 1μm the sky is comparably bright to the star, which would increase the noise in an observation by a factor of $\sim \sqrt{2}$ and would therefore decrease the S/N by the same factor. For a 10m telescope, this still indicates $S/N \sim 6$ for good seeing conditions in the situation modeled above. Note that if the plane of the planet's orbit is inclined less than 90°, then for nearly all phases the S/N for detection of the planet is reduced, for any spectral filter. The ratio of the flux from the planet through the MBF to that through the HAF, however, is independent of both inclination and phase.

Although some models of close–in extrasolar giant planets predict significantly less methane than is present in Jupiter's visible cloud-layer, this prediction is not universal. Seager, Whitney, & Sasselov (2000), for example, present a model of 51 Peg b that has spectroscopically significant methane–levels. They point out, however, that these methane features might be present only in the coolest, least absorptive models.

Even if future models should converge upon the conclusion that the gaseous methane content of hot Jupiters is very low, there are spectral features due to other chemicals that are predicted to be present in the atmospheres of close–in extrasolar giant planets, that are predicted to be comparably strong to Jupiter's methane features. A search for these other predicted features would be analogous to the methods described above. Sudarsky, Burrows, & Hubeny (2003; SBH03) identify five classes of extrasolar giant planets, ranging from class I (Jupiter–like) through classes IV ($a \sim 0.1$AU) and V ($a \sim 0.05$). A caveat introduced by SBH03 is that, for class IV and V planets, the planet's spectrum redward of ~ 500nm includes increasing levels of thermal emission, and so it makes more sense to discuss the "emergent spectrum" rather than the reflection spectrum. Their model emergent spectra for class IV planets include several strong absorption features. In the visible, sodium (~ 600nm) and potassium (~ 800nm) are predicted to induce absorption features with a comparable equivalent width to the methane features we consider above; in the NIR ($\sim 1.4\mu$m), water, which is thought to condense too deep in Jupiter to affect the cloud-top albedo, is predicted to cause an even deeper (factor of ~ 100) trough in the emergent spectrum. This water feature is at a wavelength where the Earth's sky is fairly bright (an order of magnitude or more brighter than the star), which would make it difficult to discern from ground-based observations but which should pose no difficulty for a space-based telescope. Table 1 summarizes the strengths of the three absorption features predicted in SBH03 class IV planets described above and compares them to the methane features previously considered. If a planet is detected with high S/N in a HAF but is (un)detected in a filter centered on a spectral feature with S/N much less than the number quoted in the last column of Table 1, this would be evidence for the presence of the chemical responsible for the feature.

The right-hand side of Figure 4 is summarized and generalized in Equation 7 below, which gives a rough estimation of the expected signal–to–noise for detection of a planet whose orbit is at inclination 90°, in which the source is a Main-Sequence star. The lensing configuration is taken to be the one described above. D is the diameter of the telescope's aperture, EW_f is the equivalent width of the spectral filter used, and EW_l is the equivalent width of a spectral line or feature.

$$\frac{S}{N} \sim \left(16 - \frac{\phi}{9^\circ}\right) \times \Theta(\bar{A}, D, EW_f, EW_l) \times \Psi(M_*, R_p, a) \qquad (7)$$

where Θ and Ψ are the functions given below:

$$\Theta(\bar{A}, D, EW_f, EW_l) = \frac{\bar{A}}{0.45} \times \frac{D}{10\ \mathrm{m}} \sqrt{\frac{EW_f}{150\mathrm{nm}}} \left(1 - \frac{EW_l}{EW_f}\right) \quad (8)$$

$$\Psi(M_*, R_p, a) = 10^{-3} \left(\frac{2M_*}{M_\odot} - 0.8\right) \left(\frac{R_p}{R_J}\right)^{3/2} \left(\frac{a}{1\ \mathrm{AU}}\right)^{-2}. \quad (9)$$

Observe that both Θ and Ψ are unity in the case of an R-band observation through a 10 m telescope of the planetary system considered above.

Equation 7 slightly over-predicts S/N for filters on the red side of R-band and slightly under-predicts S/N for filters on the blue side; furthermore, as above, it does not include sky-brightness, which is particularly important redward of 1μm.

7. CONCLUSIONS

In the Galactic bulge there is a large number of stars and, presumably, a comparably large number of planets. With current and future microlensing surveys in the direction of the bulge, we expect that some solar systems will cross the fold-caustics of binary lenses. Unfortunately, although in such events there will be two caustic–crossings, it appears that current technology will only allow for detection of a planet orbiting the source-star during the egress caustic–crossing – and furthermore only when the star-planet system is in the favorable configuration. Still, with its expected mean albedo, the planet should reflect enough light that, in the case we consider, it should be detectable for roughly 1/4 of its orbit with a 10m telescope.

TABLE 1

ABSORPTION FEATURES[a]

Spectral Feature	SBH03 Class	Line Center	Eq. Width	S/N Ratio
Sodium	IV	~ 600nm	~ 80nm	14
Potassium	IV	~ 780nm	~ 20nm	7
Methane	I	~ 990nm	~ 20nm	5
Methane	I	$\sim 1.00\mu$m	~ 40nm	7
Water	IV	$\sim 1.40\mu$m	~ 200nm	N/A

[a] This table shows the line-center and equivalent width for each of 5 spectral features. Three of these features, the Sodium (Na), Potassium (K), and Water features, are expected in planets classified by SBH03 as class IV ($a \sim 0.1$AU). The other two features are the methane features considered in detail in this paper, with data taken from Jupiter's reflection spectrum, available in Karkoschka (1994). The last column shows the predicted S/N ratio given the absence of the chemical, and for Na and K it is computed from Equation 7 (using $\bar{A} = 0.35$ and $EW_l = 0$), while for the Methane features it is computed from our simulations. This ratio is not applicable to the case of water, because the sky is too bright for ground-based observations at this wavelength.

Our results suggests that the strategy outlined by GG00 and Lewis & Ibata should be viable: each time a bulge star is seen to cross a fold-caustic into the ICR, the egress event should be closely monitored in order to detect a planet in the trailing (favorable) configuration, should such a favorable orientation occur. If 10% of bulge stars have hot Jupiter companions, then, since a quarter of planet-star systems will be have appropriate in the planet-trailing configuration on egress, $\sim 2-3\%$ of bulge stars that cross fold-caustics will be seen, under close monitoring (in $\sim$ 8–min integrations) during the egress crossing, to have planetary companions.

If such planets are detected, it will be possible, in principle, to determine various properties of the planet, including physical (reflectance model, phase, angular orientation relative to the caustic, presence of moons or rings; see GCH03) and chemical characteristics (the presence of specific constituent compounds of the atmosphere, as suggested by our results). Since the expected perturbations to an observed light–curve from the physical characteristics are either small (moons, rings, angular orientation) or degenerate with other effects on the total brightness of the planet, such as the planet's albedo or the solid angle it subtends from the perspective of its star (reflectance model, phase), it will be difficult in practice to determine these physical characteristics. For example, if we were to observe the egress caustic-crossing light–curve of a planet in the bulge that has rings around it, is at illumination phase $\phi = 45°$, and obeys Lommel-Seeliger reflection, we would most likely not be able to infer the presence of the rings, the phase, or the nonuniform reflectance because the data could be fit equally well (within error bars) by a best-fit $\phi = 0°$ model with no rings (at $\phi = 0°$, a Lommel-Seeliger planet is uniformly illuminated). The expected perturbations from some atmospheric compounds, however, are much greater (a factor of $\sim$ 5 or more) and do not suffer from analogous geometrical degeneracies.

In our example, using 8–minute observations on a 10m telescope, we found that the presence of methane could be inferred from a non–detection of the planet in the strong broad methane absorption band at $\approx 0.9\mu$m, accompanied by a $S/N \sim 10$ detection in adjacent bands. Observations such as the ones described in this paper will provide a crucial constraint on models of roaster atmospheres. Then, in turn, as more accurate atmosphere models become available, this S/N could improved by fitting the data to spectral templates with free parameters corresponding to variable compositions. Future generations of large telescopes might therefore be able to probe the composition of the atmospheres of distant extrasolar planets.

We thank Scott Gaudi for extremely helpful discussions and criticism, Erich Karkoschka for providing planetary albedo data, and Sara Seager for commentary on theoretical hot Jupiter atmospheres. We also thank our referee, David Graff, for suggesting many improvements upon the original version of this paper.

APPENDIX

In this Appendix, we present the specifics of our model of the planet, including details regarding the three reflectance models we consider.

The viewing geometry of a planet–star binary can be described in a three–dimensional coordinate system, centered on the planet, as illustrated in Figure 8. The z–axis is defined to point toward the observer; the x–axis is in the direction from the planet to the star, as projected on the sky from the perspective of the observer; and the y–axis is defined by the x and z-axes and the usual right–hand rule. The phase is as defined in Section 2.1 given by the angle.

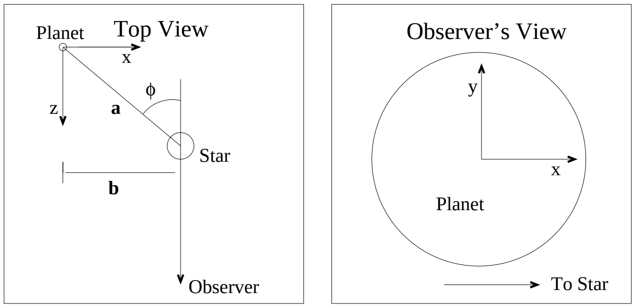

FIG. 8.— *Left panel:* Top view ("God's eye view") of the viewing geometry, showing the phase angle (ϕ), the orbital radius (a), and the projected impact parameter ($b = a\sin\phi$). *Right panel:* Observer's view of the planet.

The reflectance models considered are the following: *Uniform reflection:* the planet has uniform surface–brightness as seen from the observer, regardless of phase. *Lambert reflection:* the surface–brightness of a patch of projected surface is proportional to the cosine of the angle between the incident radiation and the surface–normal vector: $B \propto \cos(\theta_{\rm ill.})$. Let $\hat{x}$, $\hat{y}$, and $\hat{z}$ be the dimensionless coordinates on the planetary surface ($\hat{x} = x/R_p$; $\hat{y} = y/R_p$, and $\hat{z} = z/R_p$, where R_p is the planet's radius). The unit vector to the star is $\mathbf{s} = (\sin\phi, 0, \cos\phi)$, and the unit surface-normal vector is $\mathbf{N} = (\hat{x},\hat{y},\hat{z}) = (\hat{x},\hat{y},\sqrt{1-(\hat{x}^2+\hat{y}^2)})$, so the desired cosine is given by $\mathbf{s}\cdot\mathbf{N} = \hat{x}\sin\phi+\sqrt{1-\hat{x}^2-\hat{y}^2}\cos\phi$. A failing of the Lambert reflectance model is that in the "full-moon" phase, the specific intensity from the edge of the projected disk drops to zero, in conflict with the appearance of the Moon and other planets in our Solar system. *Lommel–Seeliger reflection* is a phenomenological model, designed to reproduce the reflectance of the Moon, that also mimics well the appearances of a number of other bodies in the Solar System. Neither the Lambert nor the Lommel–Seeliger model – and certainly not the uniform model – can capture in detail the appearance of a patch of planetary or Lunar surface at high resolution; but the Lommel-Seeliger model in particular is successful at reproducing at low resolution the whole planetary disk. The surface–brightness of a patch of projected surface in the Lommel-Seeliger model is proportional to the cosine of the illumination angle, and inversely proportional to the sum of the cosines of the illumination angle and the viewing angle: $B \propto \cos(\theta_{\rm ill.})/[\cos(\theta_{\rm ill.})+\cos(\theta_{\rm view})]$. The cosine of the viewing angle is the dot product of $\mathbf{N}$ with the unit vector to the observer, $\mathbf{z} = (0,0,1)$, or $\mathbf{N}\cdot\mathbf{z} = \sqrt{1-(\hat{x}^2+\hat{y}^2)}$.

Within our coordinate system, the un–magnified flux from a patch of surface at projected coordinates $(\hat{x},\hat{y})$ can be represented as follows

$$dF = KP\frac{B(\hat{x},\hat{y})}{4\pi r^2}d\hat{x}\,d\hat{y}. \tag{10}$$

Here P is the total incident stellar power that the planet reflects, or $L_*A(\pi R_p^2)/4\pi a^2$, where L_* is the luminosity of the star; A and a are the planet's albedo and orbital semi-major axis, respectively; $B(\hat{x},\hat{y})$ gives the spatial dependence of the apparent brightness of the planet, and depends on the reflectance model; r is the distance of the observer from the system; and K is an overall scale-factor so that the total reflected light equals the total intercepted light times the albedo A. What remain to be given, then, are K and B for each reflectance model.

The resulting constants and formulae are:

$$K_U = 2/\pi$$
$$K_L = 4/\pi$$
$$K_{LS} = 1.556, \tag{11}$$

and

$$B_U(\hat{x},\hat{y}) = 1$$
$$B_L(\hat{x},\hat{y}) = \hat{x}\sin\phi + \sqrt{1-(\hat{x}^2+\hat{y}^2)}\cos\phi$$
$$B_{LS}(\hat{x},\hat{y}) = \frac{\hat{x}\sin\phi + \sqrt{1-(\hat{x}^2+\hat{y}^2)}\cos\phi}{\hat{x}\sin\phi + \sqrt{1-(\hat{x}^2+\hat{y}^2)}(\cos\phi+1)}, \tag{12}$$

where the U, L, and LS subscripts refer to uniform, Lambert, and Lommel-Seeliger reflectance, respectively.

REFERENCES

Albrow, M. D. et al., ApJ, 522, 1011
Ashton, C. E., & Lewis, G. F. 2001, MNRAS, 325, 305
Bond, I. A. et al., ApJ, 606L, 155
Burrows, A. Sudarsky, D., Hubeny, I. 2004, ApJ, 609, 407
Castro, S. et al., ApJL, 548:L197
Charbonneau, D., Brown, T. M., Noyes, R. W., Gililand, R. L. 2002, ApJ, 568, 377
Efford, N., D. 1991, EM&P, 54, 19
Gaudi, B. S., Chang, H-Y., Han, C. 2003, ApJ, 586, 527 [GCH03]
Gould, A., Loeb, A. 1992, ApJ, 396, 104
Graff, D. S., Gaudi, B. S. 2000, ApJ, 538L, 133 [GG00]
Heyrovsky, D., Loeb, A. 1997, ApJ, 490, 38
Karkoschka, E. 1994, Icar., 111, 174
Keyser, R., & Witt, H. J. 1989, A&A, 221, 1
Kutchner, M. J. & Traub, W. A. 2002, ApJ, 570, 900
Leinert, Ch., et al., 1998, A&AS, 127, 1
Lewis, G. F., & Belle, K. E. 1998, MNRAS, 297, 69
Lewis, G. F., & Ibata, R. A. 2000, ApJ, 539, L63
Mao, S., Paczynski, B. 1991, ApJ, 374L, 37
Marcy, G. W., Butler, R. P. et al. 1997, ApJ, 481, 926
Marcy, G. W., Butler, R. P. 1998, ARAA, 36, 57
Oppenheimer, B. R., et al. 2001 AJ, 121, 2189
Seager, S., Whitney, B. A., Sasselov, D. D. 2000 ApJ, 540, 504
Silva, D. R., Cornell, M. 1992, ApJS, 81, 865
Sudarsky, D., Burrows, A., Hubeny, I., 2003, ApJ, 588, 1121
Vidal-Madjar, A., Lecavelier des Etangs, A., Désert, J.-M., Ballester, G. E., Ferlet, R., Hébrard, G., Mayor, M. 2003, Nature, 422, 143
Wolszczan, A., Frail, D. 1992, Nature, 355, 145
Woolf, N., Angel, J., R. 1998, ARAA, 36, 507